Published in final edited form as:
Adv Healthc Mater. 2014 November ; 3(11): 1869–1876. doi:10.1002/adhm.201400095.

Biphasic Ferrogels for Triggered Drug and Cell Delivery

Christine A. Cezar,
Harvard School of Engineering and Applied Sciences, Cambridge, MA, 02138, USA Wyss Institute for Biologically Inspired Engineering, Cambridge, MA, 02138, USA

Stephen M. Kennedy,
Harvard School of Engineering and Applied Sciences, Cambridge, MA, 02138, USA Wyss Institute for Biologically Inspired Engineering, Cambridge, MA, 02138, USA

Manav Mehta,
Harvard School of Engineering and Applied Sciences, Cambridge, MA, 02138, USA Wyss Institute for Biologically Inspired Engineering, Cambridge, MA, 02138, USA

Julius Wolff Institute, Charité - Universitätsmedizin Berlin and Berlin-Brandenburg Center for Regenerative Therapies, 13353, Berlin, Germany

James C. Weaver,
Harvard School of Engineering and Applied Sciences, Cambridge, MA, 02138, USA Wyss Institute for Biologically Inspired Engineering, Cambridge, MA, 02138, USA

Luo Gu,
Harvard School of Engineering and Applied Sciences, Cambridge, MA, 02138, USA Wyss Institute for Biologically Inspired Engineering, Cambridge, MA, 02138, USA

Herman Vandenburgh, and
Brown University Department of Pathology and Lab Medicine, Providence, RI, 02912, USA

David J. Mooney
Harvard School of Engineering and Applied Sciences, Cambridge, MA, 02138, USA Wyss Institute for Biologically Inspired Engineering, Cambridge, MA, 02138, USA

David J. Mooney: mooneyd@seas.harvard.edu

Abstract

Ferrogels are an attractive material for many biomedical applications due to their ability to deliver a wide variety of therapeutic drugs on-demand. However, typical ferrogels have yet to be optimized for use in cell-based therapies, as they possess limited ability to harbor and release viable cells. Previously, we have demonstrated an active porous scaffold that exhibits large deformations under moderate magnetic fields, resulting in enhanced biological agent release. However, at small device sizes optimal for implantation (e.g., 2 mm thickness), these monophasic ferrogels no longer achieve significant deformation due to a reduced body force. In this study, we present a new biphasic ferrogel containing an iron oxide gradient capable of large deformations

Correspondence to: David J. Mooney, mooneyd@seas.harvard.edu.

Supporting Information
Supporting Information is available online from the Wiley Online Library or from the author.

and triggered release even at small gel dimensions. Biphasic ferrogels demonstrate increased porosity, enhanced mechanical properties, and potentially increased biocompatibility due to their reduced iron oxide content. With their ability to deliver drugs and cells on-demand, it is expected that these ferrogels will have wide utility in the fields of tissue engineering and regenerative medicine.

Keywords

magnetic hydrogels; stimuli responsive; controlled delivery; cell therapy

1. Introduction

Ferrogels have potential wide utility in the medical industry as remotely controlled drug delivery devices, sensors, and actuators. These magnetic field responsive materials are typically composed of a polymer matrix with embedded iron oxide particles, often magnetite or maghemite. Upon application of a non-uniform magnetic field, the magnetic particles align with the field and move toward the region of highest field intensity. A deformation in the ferrogel is created as the surrounding polymer matrix moves together with the magnetic particles, resulting in fluid convection and enhanced drug release. In this way, bioagent release can be easily triggered from the device in a noninvasive and precisely timed manner. A variety of polymers, particle concentrations, and gel porosities have been previously investigated leading to ferrogels with vastly different material properties and triggered release capabilities.[1–9]

Although ferrogels are often designed with biomedical applications in mind, typical ferrogels have yet to be optimized for use as implantable biomaterials. In addition to controlled drug release, it is important for tissue engineering scaffolds to be able to harbor and release cells so that they can be used for cell-based regenerative therapies. However, the vast majority of ferrogels possess significant limitations that render them unsuitable for cell survival or delivery. For example, many ferrogels possess pores smaller than typical cells[2, 3, 7] or rely on controlled drug permeation to trigger release.[1, 4, 6] These gels exhibit a closed configuration, a diffusive release mechanism, and decreased release in the presence of a magnetic field due to a physical collapse of the structure. This mechanism of release severely limits nutrient transport and convection within the ferrogel for extended periods of time. Additionally, some ferrogel formulations require iron oxide concentrations greater than 15 wt% for optimal magnetic sensitivity,[1, 6] increasing the risk of toxicity upon subcutaneous implantation as this concentration approaches a lethal dose in mice.[10] Equally important, at these high iron oxide concentrations, cells within the ferrogel may be sensing a much stiffer material than intended, potentially leading to unwanted changes in cell fate.[11–13] Previously, we have demonstrated an active porous scaffold that can be remotely controlled by a magnetic field to deliver various biological agents, including cells, on demand.[8] This ferrogel scaffold, a macroporous alginate ferrogel containing 13 wt% iron oxide nanoparticles, demonstrates significant deformations (>70%) and release under moderate magnetic fields at large gel dimensions.

This alginate-iron oxide material system is particularly attractive for biomedical applications due to the previous clinical use of iron oxide particles as magnetic resonance imaging contrast agents, as well as, the biocompatibility, low toxicity, and extensive use of alginate as a drug delivering biomaterial.[14, 15] Here we have performed studies to determine how these alginate-iron oxide ferrogels function after they are scaled down to a size more appropriate for biomedical testing in rodents. At small dimensions (e.g. 2 mm thickness), implantation is simple, but the significant deformation and release exhibited by the larger ferrogels may be challenging to achieve due to the reduced iron oxide content available to generate a body force, the reduced magnetic field gradient visible to the particles, and the reduced pore size associated with the fabrication of smaller gels. In order to address these potential issues, iron oxide content was spatially redistributed into a distinct compartment within the small ferrogel, creating a new biphasic ferrogel.

2. Results and Discussion

2.1 Monophasic Ferrogels – Particle Size and Device Miniaturization

In order to compare the ability of iron oxide particles of varying size to induce a maximal ferrogel response upon magnetic field stimulation, large monophasic ferrogels with homogenous particle distribution were fabricated using alginate and iron oxide as previously described.[8] When subjected to a moderate vertical magnetic field gradient, ferrogels fabricated with larger iron oxide particles (<5 μm) exhibited significantly greater deformation (>40%) and model drug (mitoxantrone) release when compared to ferrogels fabricated with smaller iron oxide particles (<50 nm) (Figure 1A, B, C). The discrepancy in deformation observed between the two particle sizes likely results largely from structural defects and finite-size effects developed during particle synthesis.[16, 17] Transmission electron microscopy (TEM) imaging revealed the larger particles to be irregular in shape suggesting they originated from ground bulk material, while the smaller particles appeared spherical indicating they were chemically synthesized as nanoparticles (Figure 1D).[17] Additionally, it has been shown that saturation magnetization values of iron oxide generally decrease with decreasing particle size.[18, 19] Differences in particle chemical composition observed during powder X-ray diffraction (XRD) studies may also partially account for differences in magnetic properties (Figure S1). Although both powders were purchased as magnetite, XRD analyses suggested that the larger particles were mainly composed of magnetite while the smaller particles were mainly composed of maghemite, a form of iron oxide with a bulk saturation magnetization significantly lower than that of magnetite.[20] Consequently, in order to maximize ferrogel deformation and bioagent release, the more responsive larger iron oxide particles were chosen for further device miniaturization studies.

While large monophasic ferrogels fabricated with the larger iron oxide particles exhibited substantial deformations, these ferrogels did not adequately perform when miniaturized. Small monophasic ferrogels (2 mm height, 8 mm diameter) exhibited a significantly reduced deformation when compared to large monophasic ferrogels (15 mm height, 20 mm diameter) of the same iron oxide concentration (Figure 1E, F). Ferrogel deformation decreases with reduction of device size, in part, because less iron oxide content is available to generate a body force in smaller systems. However, simply supplementing smaller ferrogels with

additional iron oxide tends to stiffen the matrix and decrease magnetic field driven gel compression.[6, 21] Additionally, small ferrogels experience a reduced field gradient within their volume when compared to large systems subject to the same magnetic field, leading to a smaller body force that may not be sufficient to produce the same degree of deformation achieved in larger systems. With these considerations in mind, the material was redesigned in order to achieve significant deformation in small ferrogels with a moderate magnetic field.

2.2. Biphasic Ferrogel Fabrication and Characterization

2.2.1 Fabrication—We hypothesized that removing iron oxide from the deforming portion of the gel, thereby reducing gel stiffness and increasing porosity, and redistributing it atone side of the gel distant from the magnetic source would significantly improve small ferrogel deformation and bioagent release. Small biphasic ferrogels containing an iron oxide gradient were fabricated using a simple polymerization (covalent crosslinking) and freeze-drying technique, similar to that used for monophasic ferrogels (Figure 2A).[8] The biphasic ferrogel iron oxide gradient, formed during polymerization in the presence of a non-uniform magnetic field, was visible using scanning electron microscopy (SEM) with energy dispersive spectroscopy (EDS)(Figure 2B). Aligned iron oxide particles formed visible columns that penetrated down into the pure alginate region of the ferrogel (Figure 2C, ii–iv). These columnar structures, composed of particles aligned with the applied magnetic field, were permanently fixed into the gel through crosslinking, resulting in a material with magnetic anisotropy.[22] Previously, this technique has been used to create uniaxial magnetic gels with frozen-in magnetic order by polymerizing ferrogels in the presence of a uniform magnetic field.[23, 24] Interconnected macropores were created by freezing the ferrogels, covalently crosslinked with adipic acid dihydrazide, at −20°C and lyophilizing.[25] Biphasic and monophasic ferrogels exhibited significantly different porosities, with large pores (340 μm) of high interconnectivity (80% open porosity) in biphasic alginate rich regions, small pores (140 μm) of reduced interconnectivity (71% open porosity) in biphasic iron oxide rich regions, and intermediate pores (160 μm) of reduced interconnectivity (64% open porosity) in monophasic ferrogels (Figure 2D, 2E). Increasing iron oxide content relative to polymer concentration decreases swelling caused by water, and consequently macropore size and interconnectivity, due to the reinforcement the iron oxide imparts to the gel.[6, 26, 27] Importantly, both monophasic and biphasic ferrogel pore sizes fall within the 100 to 500 μm range suggested for optimal cell survival.[28] However, due to the larger pore size and increased interconnectivity of their alginate rich region, biphasic ferrogels are expected to offer enhanced drug delivery with lower iron oxide content and improved cell seeding efficiency and triggered release.[25]

2.2.2. Deformation—The ability of biphasic ferrogels to demonstrate large and rapid deformations at small device sizes ideal for implantation was investigated. When compared to monophasic ferrogels of the same size, shape, and iron oxide concentration, small biphasic ferrogels exhibited a significantly increased deformation at all iron oxide concentrations examined, with nearly all biphasic conditions demonstrating greater than a 2.4-fold increase (Figure 3A, 3B, Video S1). This enhancement in biphasic ferrogel deformation, likely resulting from both iron oxide redistribution and increased macropore

size, was also observed with ferrogels subjected to other magnetic surface field intensities (Figure S2). Importantly, small biphasic ferrogels were able to maintain the very rapid and large deformation observed with conventional monophasic ferrogels but with significantly reduced iron oxide content. As expected, the large deformation exhibited by biphasic ferrogels translated into an enhanced mitoxantrone release rate over unstimulated controls (54–81 fold increase) at all iron oxide concentrations and over monophasic ferrogels (1.4–2.0 fold increase) at the low iron oxide concentrations attractive for in vivo work (Figure S3, 3C). However, at high iron oxide concentrations, an increase in deformation did not directly correspond to an increased drug release rate. While the highly porous alginate rich region comprised a large percentage of the total biphasic ferrogel volume at low iron oxide concentrations, it constituted a relatively small portion at high iron oxide concentrations, lowering the average porosity of the gel and likely decreasing drug diffusion and free mitoxantrone as the iron oxide rich ferrogel walls become more abundant (Figure S4). Nevertheless, the maximal triggered drug release rate from biphasic ferrogels was found within a wider range of iron oxide particle concentrations (2 to 7 wt%) than the range demonstrated by monophasic ferrogels. Due to their optimal release rate and deformation, 7 wt% biphasic ferrogels were chosen for subsequent cell studies, as large deformations and resulting fluid convection are required for maximal cell release.[8]

2.2.3. Mechanical Testing—Small biphasic ferrogels were mechanically tested in order to determine whether they balance a large deformation and minimal iron oxide content with desirable gel mechanics. Biphasic ferrogels were significantly softer than monophasic ferrogels above 3 wt% iron oxide. While gel stiffness increases with iron oxide content in a monophasic system, iron oxide concentration did not significantly affect the bulk Young's modulus of biphasic ferrogels (Figure 4A, 4B, 4C).[6, 21] As a result, ferrogel iron oxide content can be optimized without significantly altering the mechanics associated with the alginate rich region of the gel, allowing the stiffness of the gel to be controlled in a more conventional manner by altering polymer concentration and crosslinking density.[29, 30] This is especially appealing for cell delivery applications as direct contact between cells and iron oxide particles in the gel is minimized, reducing the risk of unwanted alterations in cell behavior, such as proliferation and differentiation, that may result from mechanosensing the particles.[11–13] Additionally, biphasic ferrogels also exhibited enhanced fatigue resistance when subjected to extensive cyclic mechanical testing. Cyclic compressions simulate the deformation triggered by the repeated magnetic field application required for efficient bioagent release. Biphasic ferrogels demonstrated a lower change in Young's Modulus, toughness (measured at 50% strain), and energy absorbed (measured at 50% strain) from the first cycle to the four thousandth cycle when compared to monophasic ferrogels of the same iron oxide concentration, indicating enhanced fatigue resistance (Figure 4A, 4B, 4D, 4E, S5). This ability to withstand repeated large deformations is likely to be critical for the success of these ferrogels as an implantable drug delivery device, but cyclic fatigue testing is only rarely included in the mechanical characterization of magnetically responsive biomaterials.

2.3. Biphasic Ferrogel Bioagent Release

2.3.1. Model Drug Release – Mitoxantrone—The on-demand drug release capabilities of small biphasic ferrogels were explored next. Mitoxantrone, an antineoplastic agent, was chosen as a model drug due to its ability to interact ionically with alginate and exhibit delayed release.[31] Cumulative mitoxantrone release from biphasic ferrogels increased with decreased iron oxide content, a potential advantage for in vivo applications (Figure 5A). As iron oxide content is decreased, the highly porous alginate rich region occupies an increased percentage of the total biphasic ferrogel volume, leading to an increased amount of iron oxide free macropore walls (Figure S4). Diffusion within these alginate rich walls is likely enhanced, leading to improved triggered and diffusive drug release. This potential increase in diffusive release may prove especially advantageous for high molecular weight or highly charged drugs that are more difficult to deliver.[32] Drug release profiles for monophasic and biphasic ferrogels were fairly equivalent at 7 wt% iron oxide. However, biphasic ferrogels offered a broader range of cumulative therapeutic doses (65 μg to 95 μg) than monophasic ferrogels (70 μg to 85 μg) when iron oxide content was varied from 2 wt% to 13 wt% (Figure 5A, 5B), indicating biphasic ferrogels provide highly tunable drug release beyond that achievable with a monophasic system.

2.3.2 Cell Release – Primary Myoblasts—In order to determine the ability of biphasic ferrogels to harbor viable cells and provide on-demand cell delivery, ferrogels containing RGD-modified alginate were created. The covalent modification of alginate with the cell adhesion ligand RGD allows cells to recognize and interact with alginate matrices.[33] This is essential for the viability of anchorage dependent cells, such as normal epithelial and endothelial cells, that require integrin binding for survival.[34] Following two days of magnetic field stimulation, biphasic ferrogels delivered more than twice the amount of viable cells as monophasic ferrogels of the same iron oxide concentration (Figure 5C, Table S1). Interestingly, the viability of cells released from biphasic ferrogels remained greater than 80± 10% throughout the stimulation period while the viability of cells released from monophasic ferrogels decreased from 60± 10% at 24 hours to 40± 20% at 48 hours. The increased deformation offered by biphasic ferrogels over their monophasic counterparts likely allows for a convective flow through the scaffold that leads to maximal cell release. Cell release was further tailored by altering the density of RGD ligands presented to the cells from the gel. Increasing the RGD density increases the adhesiveness of the material without altering its stiffness (Figure S6).[35, 36] As expected, maximal cell release was achieved with a minimally adhesive material, a RGD density of one peptide per alginate chain (DS1) (Figure 5D). DS1 biphasic ferrogels were able to deliver 1.4×10^5 viable cells in two days, a quantity within the same order of magnitude as those typically used to seed tissue engineering scaffolds prior to implantation.[37–39] Additionally, cell delivery from biphasic ferrogels does not rely upon the outward migration of the cells from the scaffold as it does in many conventional scaffold systems, a potential benefit of using this on-demand cell delivery strategy for regenerative cell therapies.

2.4. Biphasic Ferrogel Implantation

Finally, the *in vivo* response to biphasic ferrogel scaffolds was investigated in a preliminary study. Due to their small size, biphasic ferrogels could undergo successful implantation

within relatively constricted areas in small animal models. Biphasic ferrogels were surgically implanted subcutaneously in the hindlimb of six week old mice, with iron oxide rich regions contacting the skin and alginate rich regions contacting the muscle tissue (Figure 6A). Orientation of the implant in this manner minimizes contact between iron oxide and the potential site of injury, possibly eliminating any further inflammation caused by iron oxide in the gel. At the time of retrieval, 3 days and 2 weeks following implantation, all scaffolds remained localized at the initial implant site. Biphasic ferrogels remained largely free of cells, indicating the gels did not induce a large inflammatory response (Figure 6B, 6C). At 2 weeks, a thin fibrous capsule was seen surrounding the implant, but the scaffolds remained largely a cellular suggesting that biphasic ferrogels are largely biocompatible and would be a useful scaffolding system for many tissue engineering applications.

3.Conclusions

By redistributing the iron oxide content of the conventional monophasic ferrogel, we were able to fabricate biphasic ferrogels appropriate in size and mechanical properties for in vivo implantation and on-demand triggered release in small animal models. With these small biphasic ferrogels we were able to achieve maximum deformations comparable to those achieved by much larger monophasic ferrogels, but with significantly reduced iron oxide content and potentially increased biocompatibility. Due to their enhanced ability to release drugs and cells on-demand, we believe these small biphasic ferrogels will have wide utility for tissue regeneration and cell therapies. More broadly, this biphasic ferrogel design can likely be applied to other polymer-magnetic material composites that may enable small scale devices in other fields including magnetoactive microfluidic valves.[40]

4. Experimental Section

Materials

High molecular weight (~250 kDa) sodium alginate with high guluronate content (ProtanalLF20/40) was purchased from Pronova Biopolymers (Oslo, Norway). Alginates were used following covalent RGD modification and dialysis purification, as previously described.[33] Ham's F10 media and DPBS containing calcium chloride and magnesium chloride were purchased from Invitrogen (Carlsbad, CA). Media supplements bFGF (Peprotech, Rocky Hill, NJ), FBS (Gibco, Grand Island, NY), BSA (Roche, Basel, Switzerland), and Trypan Blue (Gibco) were used for cell release experiments. Iodixanol solution used for micro-CT contrast was purchased from US Pharmacopeia (Rockville, MD). All other chemicals including adipic acid dihydrazide (AAD), 1-ethyl-3-(dimethylaminopropyl) carbodiimide (EDC), MES, 1-hydroxybenzotriazole (HOBT), Iron (II, III) oxide powder (<5 μm, Cat. No. 310069), Iron (II, III) oxide nanopowder (<50 nm, Cat. No. 637106), and mitoxantrone were purchased from Sigma-Aldrich (St. Louis, MO). It is important to note that Iron (II, III) oxide powder (<5 μm) and nanopowder (<50 nm) were purchased from Sigma-Aldrich as magnetite (Fe_3O_4), but powder x-ray diffraction data reveal that the nanopowder is likely composed of maghemite (Fe_2O_3) (Figure S1).

Monophasic and Biphasic Ferrogel Fabrication

To create monophasic ferrogels, alginate in MES buffer (0.1 m MES and 0.5 m NaCl, pH 6.0) containing HOBT and AAD was sequentially mixed with an aqueous solution of iron oxide particles and EDC (0.1 g/ml). The resulting solution of alginate (1 wt%), iron oxide particles (2–13 wt%), and AAD (2.5 mm) was immediately cast between two glass plates separated by 2–3 mm spacers and allowed to polymerize for 3 hours. To create biphasic ferrogels, the solution was subjected to a vertical magnetic field gradient, generated by a magnet with a surface field of 6510 Gauss (K&J Magnetics, Cat. No. DX0Z0), during polymerization. The resulting ferrogels were then cut into 8 mm diameter disks using a biopsy punch. Ferrogel disks were washed in a large volume of distilled water for 48 hours to remove residual reagents, frozen overnight at −20°C, and lyophilized.

Electron Microscopy Sample Preparation

SEM samples were prepared by dehydration in ethanol followed by critical point drying and Pt/Pd sputter coating. Structural and compositional analyses of the ferrogels were performed with a Tescan Vega Environmental SEM equipped with a Bruker XFlash 5030 Energy Dispersive Spectrometer. Backscattered electron imaging and elemental mapping of carbon and iron for each sample were performed under identical conditions at an accelerator voltage of 20 keV and a chamber pressure of 12 Pa. To acquire TEM images of iron oxide particles, the samples were suspended in ethanol, dried on copper grids, and imaged with a JEOL 2100 TEM.

Pore Size and Open Porosity

Ferrogel pore structure was examined using microcomputed tomography (micro-CT). Prior to imaging, ferrogels were soaked overnight in an Iodixanol solution (200 mg/ml), frozen at −20 °C, and lyophilized. Ferrogel scaffolds were then placed in a custom-built radiolucent batch scanning acrylic tube. The scans were performed on a high resolution scanner (HMXST225, X-Tek; Nikon Metrology NV) at a voltage of 45 kV, current of 275 μA, and integration time of 1000 ms. Voxel size was selected to be isotropic and fixed at 8 μm. The images obtained from acquisition were first reconstructed to serial coronal-oriented tomograms using the manufactures 3D cone beam reconstruction algorithm. Volumetric reconstruction was done using VG studio max 2.0 (Volume Graphics GmbH, Germany) and 3D microarchitectural morphological analyses were conducted using CTAn software (SkyScan, Aartselaar, Belgium). For each scaffold, a cylindrical volume of interest (VOI) of 8 mm diameter and 2 mm height was selected and segmented using a low pass Gaussian filter. A fixed global threshold of approximately 33% attenuation of maximum pixel intensity was chosen as it allowed the rendering of scaffold material and exclusion of background noise for all ferrogel regions. Pore size was calculated from binary micro-CT images by averaging all pore diameters in each ferrogel region. Open porosity was calculated as the percentage of open pores in the total VOI volume, with open pores defined as any space located within a solid object or between solid objects, which has any connection in 3D to the space outside the object or objects.

Maximum Deformation

The height of fully hydrated ferrogel disks was measured before and after application of a magnetic field gradient generated by the same magnet used for fabrication. Maximum deformation was calculated as the percent reduction in height resulting from magnetic field stimulation.

Mechanical Testing

Fully hydrated ferrogel disks were subjected to compression tests using an Instron 3342 single column apparatus with a strain rate of 20% per minute. Engineering stresses and strains were recorded, and the Young's modulus (E) was calculated from the linear portion of the stress-strain curve according to Hooke's law: $\sigma = E\varepsilon$. For cyclic compression studies, gels were tested at a strain rate of 100% per minute and were subjected to 4000 compression cycles with a maximum strain of 50%.Mechanical compressions, rather than magnetic field triggered deformations, were performed in order to ensure a consistent strain rate and maximum strain throughout the 4000 compressions in all ferrogels tested. For each 1000^{th} compression cycle, toughness at 50% strain was calculated as the integral of the corresponding stress-strain curve shown in Figure 4A and 4B from 0 to 50% strain. Energy absorbed by the material was calculated as the difference between the integral of the stress-strain curve undergoing compression from 0 to 50% strain and the integral of the stress-strain curve undergoing decompression from 50 to 0% strain.

Controlled Mitoxantrone Release

Dry ferrogel disks with a volume of about 150 μL were allowed to fully absorb an aqueous solution of mitoxantrone (75μL, 2 mg/mL) and stored at 4°C overnight. The disks were then placed in a DPBS solution containing calcium chloride, magnesium chloride, and 1% BSA to begin release. Every 2 hours, stimulated ferrogels were subjected to 120 cycles (on/off) of magnetic field over 2 minutes, while no magnetic field was applied to control gels. The release buffer was replaced after each period of magnetic stimulation. Concentrations were determined by recording the absorbance of mitoxantrone in DPBS at a wavelength of 610 nm.

Controlled Cell Release

Ferrogel disks covalently modified with RGD peptide at a degree of substitution of 10 (DS10, 10 RGD peptides per alginate chain) were hydrated in F10 medium overnight at 37°C and 5% CO_2.[33] Media was then wicked away with a Kimwipe and 2×10^5 primary mouse myoblasts were seeded onto each gel. Cell seeding solution was completely wicked into each gel, leading to a homogenous cell distribution throughout the scaffold.[38] Gels were placed at 37°C and 5% CO_2 for 30 minutes to facilitate cell attachment. F10 media containing 20% FBS and bFGF (5 ng/ml) was then added to each gel. Every 24 hours, ferrogels were placed into fresh media and subjected to 120 cycles (on/off) of magnetic field over 2 min, while no magnetic field was applied to control gels. A strain rate of 1 Hz was chosen as it allowed for nearly complete gel recovery following deformation and minimized the time that cell seeded ferrogels were required at room temperature without 5% CO_2.Cell concentrations and viability were determined using disposable hemocytometers (Incyto) and

trypan blue. RGD density optimization experiments were carried out in a similar manner except 4×10^5 cells were seeded directly onto dry scaffolds of RGD DS1, 5, 10, and 20, and ferrogels were stimulated at 2, 24, and 48 hours.

Scaffold Implantation

All animal work was performed in compliance with NIH and institutional guidelines. Six week old female wild type C57BL/6J mice (Jackson Laboratories, Bar Harbor, ME, USA) were anesthetized with an intraperitoneal injection of ketamine (80 mg/kg) and xylazine (5 mg/kg). A biphasic ferrogel (7 wt%) hydrated with 100 μl PBS was placed subcutaneously on the tibialis anterior muscle, and the incision was surgically closed. Biphasic ferrogel scaffolds were stimulated for 5 minutes at 1 Hz every 12 hours. Following retrieval at 3 days and 2 weeks, scaffolds were fixed in 10% neutral buffered formalin overnight. Ferrogels were then paraffin embedded, sectioned at 7 μm thickness, and stained with hematoxylin and eosin at the Harvard Rodent Histopathology Core.

Statistical Analysis

All statistical comparisons were performed using ANOVA with Bonferroni's post-hoc test and a two-tailed unpaired Student's *t*-test with Welch's correction and analyzed using INSTAT 3.1a (GraphPad Software, Inc., San Diego, CA, USA) software. Differences between conditions were considered significant if $p<0.05$.

Supplementary Material

Refer to Web version on PubMed Central for supplementary material.

Acknowledgments

This work was supported by National Science Foundation Grant DMR-0820484, National Institutes of Health Grant R01 DE013349, Materials Research Science and Engineering Center (MRSEC) at Harvard University, BASF Advanced Research Initiative at Harvard University, and Department of Defense National Defense Science and Engineering Graduate Fellowship. This work was performed in part at the Center for Nanoscale Systems (CNS), a member of the National Nanotechnology Infrastructure Network (NNIN), which is supported by the National Science Foundation under NSF award no. ECS-0335765. CNS is part of Harvard University. The authors would like to thank Dr. William Croft for assistance with powder X-ray Diffraction and Dr. Roderick Bronson of the Harvard Rodent Histopathology Core for his pathological assessment of histology sections.

References

1. Liu TY, Hu SH, Liu TY, Liu DM, Chen SY. Langmuir. 2006; 22:5974. [PubMed: 16800645]
2. Satarkar NS, Hilt JZ. J. Controlled Release. 2008; 130:246.
3. Hu SH, Liu TY, Liu DM, Chen SY. Macromolecules. 2007; 40:6786.
4. Hu SH, Liu TY, Liu DM, Chen SY. J. Controlled Release. 2007; 121:181.
5. Zelis PM, Muraca D, Gonzalez JS, Pasquevich GA, Alvarez VA, Pirota KR, Sanchez FH. J. Nanopart. Res. 2013; 15
6. Liu TY, Hu SH, Liu KH, Liu DM, Chen SY. J. Controlled Release. 2008; 126:228.
7. Gonzalez JS, Nicolás P, Ferreira ML, Avena M, Lassalle VL, Alvarez VA. Polym. Int. 2014; 63:258.
8. Zhao X, Kim J, Cezar CA, Huebsch N, Lee K, Bouhadir K, Mooney DJ. Proc. Natl. Acad. Sci. U. S. A. 2011; 108:67. [PubMed: 21149682]

9. Resendiz-Hernandez PJ, Rodriguez-Fernandez OS, Garcia-Cerda LA. J. Magn. Magn. Mater. 2008; 320:E373.
10. Zhai Y, Wang XL, Wang XM, Xie H, Gu HC. J. Biomed. Mater. Res., Part A. 2008; 85A:582.
11. Engler AJ, Sen S, Sweeney HL, Discher DE. Cell. 2006; 126:677. [PubMed: 16923388]
12. Huebsch N, Arany PR, Mao AS, Shvartsman D, Ali OA, Bencherif SA, Rivera-Feliciano J, Mooney DJ. Nat. Mater. 2010; 9:518. [PubMed: 20418863]
13. Guilak F, Cohen DM, Estes BT, Gimble JM, Liedtke W, Chen CS. Cell Stem Cell. 2009; 5:17. [PubMed: 19570510]
14. Augst AD, Kong HJ, Mooney DJ. Macromol. Biosci. 2006; 6:623. [PubMed: 16881042]
15. Wang YX. Quant. Imaging Med. Surg. 2011; 1:35. [PubMed: 23256052]
16. Batlle X, Labarta A. J. Phys. D: Appl. Phys. 2002; 35:R15.
17. Tartaj P, Morales MD, Veintemillas-Verdaguer S, Gonzalez-Carreno T, Serna CJ. J. Phys. D: Appl. Phys. 2003; 36:R182.
18. Goya GF, Berquo TS, Fonseca FC, Morales MP. J. Appl. Phys. 2003; 94:3520.
19. Morales MP, Andres-Verges M, Veintemillas-Verdaguer S, Montero MI, Serna CJ. J. Magn. Magn. Mater. 1999; 203:146.
20. Dunlop, DJ.; Özdemir, Ö. Rock Magnetism: Fundamentals and Frontiers. Cambridge University Press; 2001.
21. Zrinyi M, Barsi L, Szabo D, Kilian HG. J. Chem. Phys. 1997; 106:5685.
22. Sharma N, Jaffari GH, Shah SI, Pochan DJ. Nanotechnology. 2010; 21
23. Collin D, Auernhammer GK, Gavat O, Martinoty P, Brand HR. Macromol. Rapid Commun. 2003; 24:737.
24. Varga Z, Feher J, Filipcsei G, Zrinyi M. Macromol. Symp. 2003; 200:93.
25. Thornton AJ, Alsberg E, Albertelli M, Mooney DJ. Transplantation. 2004; 77:1798. [PubMed: 15223894]
26. Galicia JA, Sandre O, Cousin F, Guemghar D, Menager C, Cabuil V. J. Phys.: Condens. Matter. 2003; 15:S1379.
27. Varga Z, Filipcsei G, Zrinyi M. Polymer. 2006; 47:227.
28. Ikada Y. J. R. Soc., Interface. 2006; 3:589. [PubMed: 16971328]
29. Kong HJ, Lee KY, Mooney DJ. Polymer. 2002; 43:6239.
30. Lee KY, Rowley JA, Eiselt P, Moy EM, Bouhadir KH, Mooney DJ. Macromolecules. 2000; 33:4291.
31. Bouhadir KH, Alsberg E, Mooney DJ. Biomaterials. 2001; 22:2625. [PubMed: 11519782]
32. Drury JL, Mooney DJ. Biomaterials. 2003; 24:4337. [PubMed: 12922147]
33. Rowley JA, Madlambayan G, Mooney DJ. Biomaterials. 1999; 20:45. [PubMed: 9916770]
34. Frisch SM, Ruoslahti E. Curr. Opin. Cell Biol. 1997; 9:701. [PubMed: 9330874]
35. Rowley JA, Mooney DJ. J. Biomed. Mater. Res. 2002; 60:217. [PubMed: 11857427]
36. Masters, KS.; Anseth, KS. Advances in Chemical Engineering, Vol. 29. Peppas, NA.; Sefton, MV., editors. Vol. Ch. 2. Academic Press; 2004.
37. Borselli C, Cezar CA, Shvartsman D, Vandenburgh HH, Mooney DJ. Biomaterials. 2011; 32:8905. [PubMed: 21911253]
38. Wang L, Shansky J, Borselli C, Mooney D, Vandenburgh H. Tissue Eng., Part A. 2012; 18:2000. [PubMed: 22646518]
39. Vacharathit V, Silva EA, Mooney DJ. Biomaterials. 2011; 32:3721. [PubMed: 21334064]
40. Hong S, Jung Y, Yen R, Chan HF, Leong KW, Truskey GA, Zhao XH. Lab Chip. 2014; 14:514. [PubMed: 24310854]

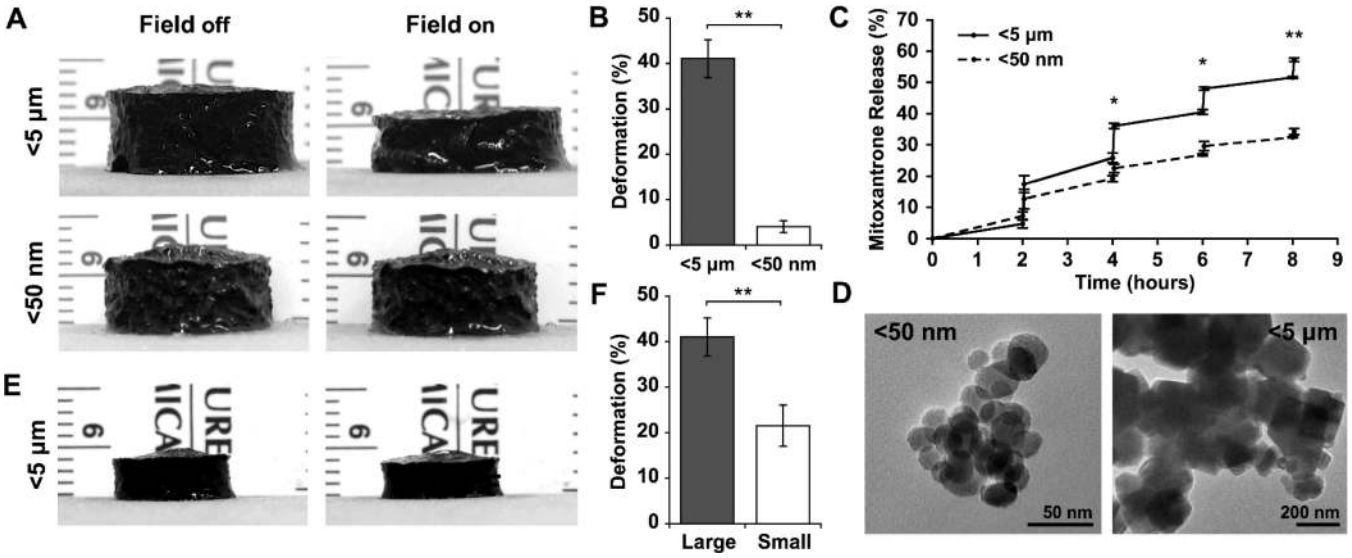

Figure 1.

(A) Photographs of large (15 mm height and 20 mm diameter) 7 wt% iron oxide monophasic ferrogels fabricated with <5 μm and <50 nm particles in the presence of no magnetic field (field off) and a moderate vertical magnetic field gradient (field on). (B) Quantified deformation of ferrogels fabricated with <5 μm and <50 nm particles during magnetic field stimulation. (C) Mitoxantrone release from ferrogels fabricated with <5 μm and <50 nm particles following magnetic stimulation for 2 minutes at 1 Hz every 2 hours. (D) Iron oxide <5 μm and <50 nm particles observed by TEM. (E) Photographs of small (2 mm height and 8 mm diameter) ferrogels fabricated with <5 μm particles in the presence of no magnetic field (field off) and a moderate vertical magnetic field gradient (field on). (F) Quantified deformation of large and small ferrogels fabricated with <5 μm particles during magnetic field stimulation. Values represent the mean and standard deviation (n = 3–6). Data were compared using a two-tailed unpaired Student's t-test with Welch's correction (*$p < 0.05$, **$p < 0.01$).

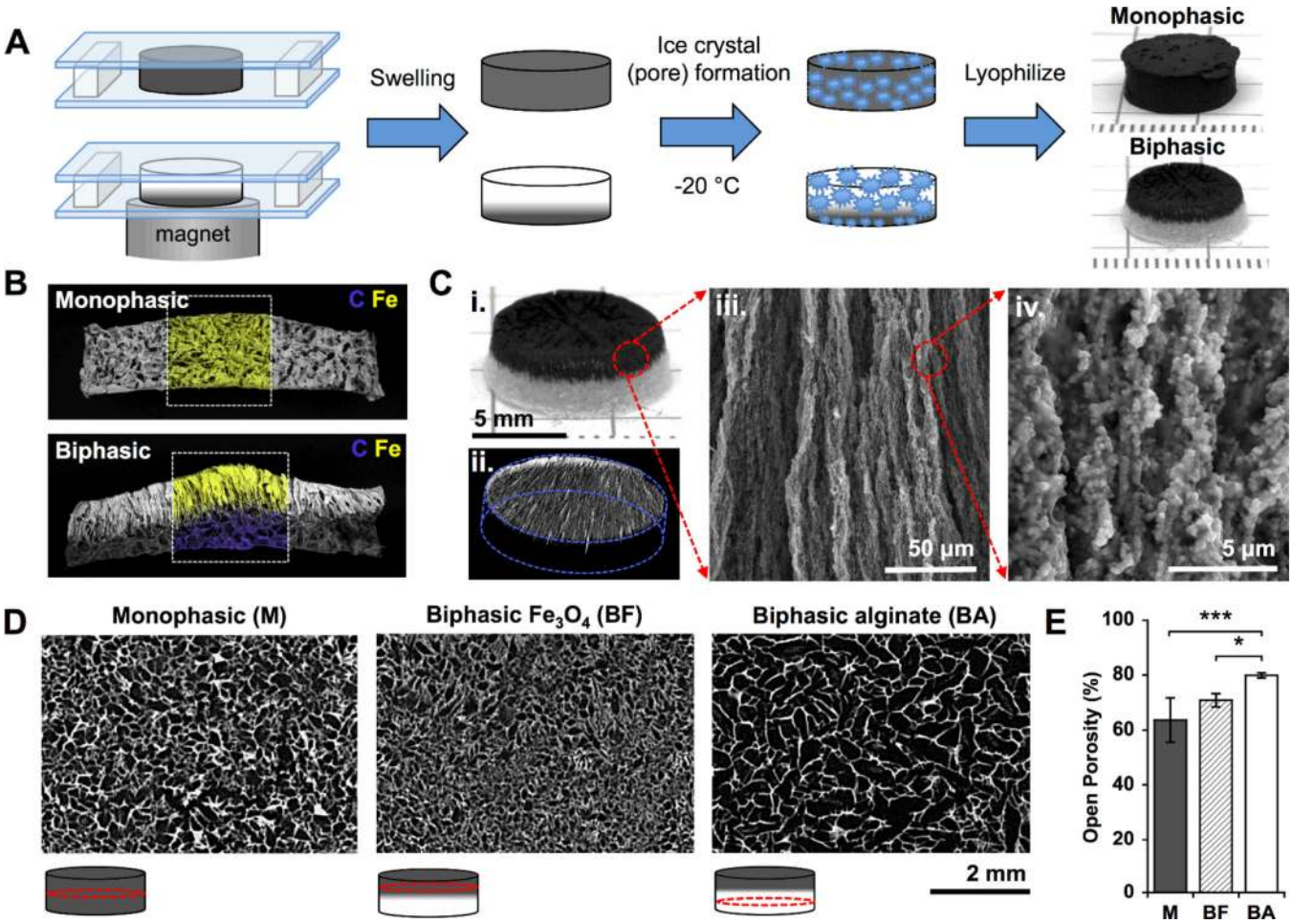

Figure 2.

(A) Schematic of monophasic and biphasic ferrogel fabrication. (B) SEM/EDS of monophasic and biphasic ferrogels showing contained iron in yellow and carbon in blue. (C) Photograph (i), micro-CT (ii), and SEM (iii and iv) images of fully fabricated biphasic ferrogels. (D) Micro-CT images showing the porosity of monophasic and biphasic ferrogels at the locations indicated by red circles in the schematic under each micro-CT image. (E) Quantified open porosity of monophasic (M), biphasic iron oxide rich (BF), and biphasic alginate rich (BA) ferrogel regions. Values represent the mean and standard deviation (n= 4). Data were compared using ANOVA with Bonferroni's post-hoc test (*$p < 0.05$, ***$p <$ 0.001).

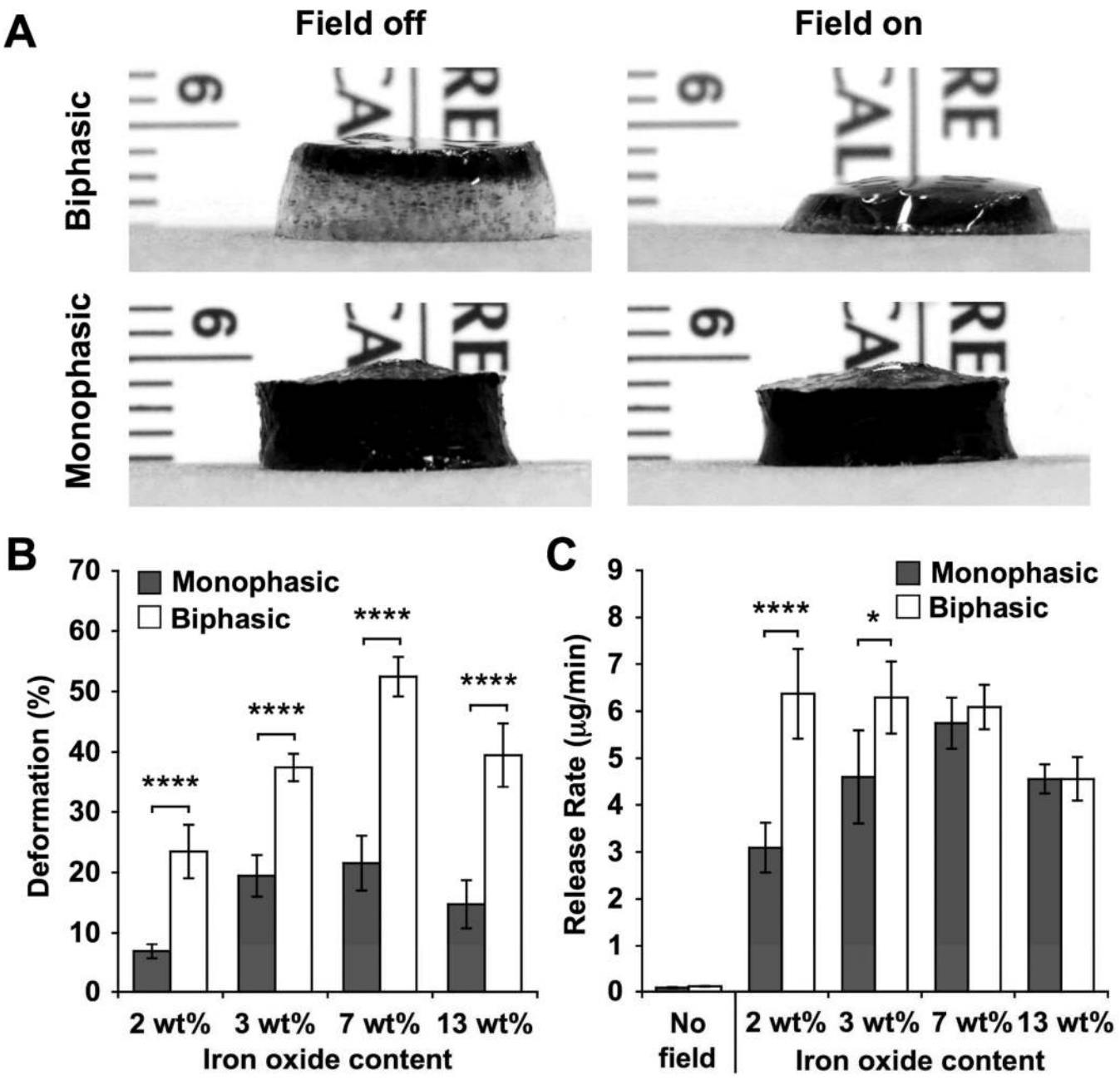

Figure 3.

(A) Photographs of small 7 wt% iron oxide biphasic and monophasic ferrogels in the presence of no magnetic field (field off) and a moderate vertical magnetic field gradient (field on). (B) Quantified deformation of small biphasic and monophasic ferrogels with varying iron oxide concentration during magnetic field stimulation. (C) Mitoxantrone release rate from small ferrogels with varying iron oxide concentration during 2 minutes of stimulation at 1 Hz. No field release rates were calculated from 3wt% unstimulated ferrogels. See Figure S3 for full data set. Values represent the mean and standard deviation (n = 4–6). Data were compared using ANOVA with Bonferroni's post-hoc test (*$p < 0.05$, ****$p < 0.0001$).

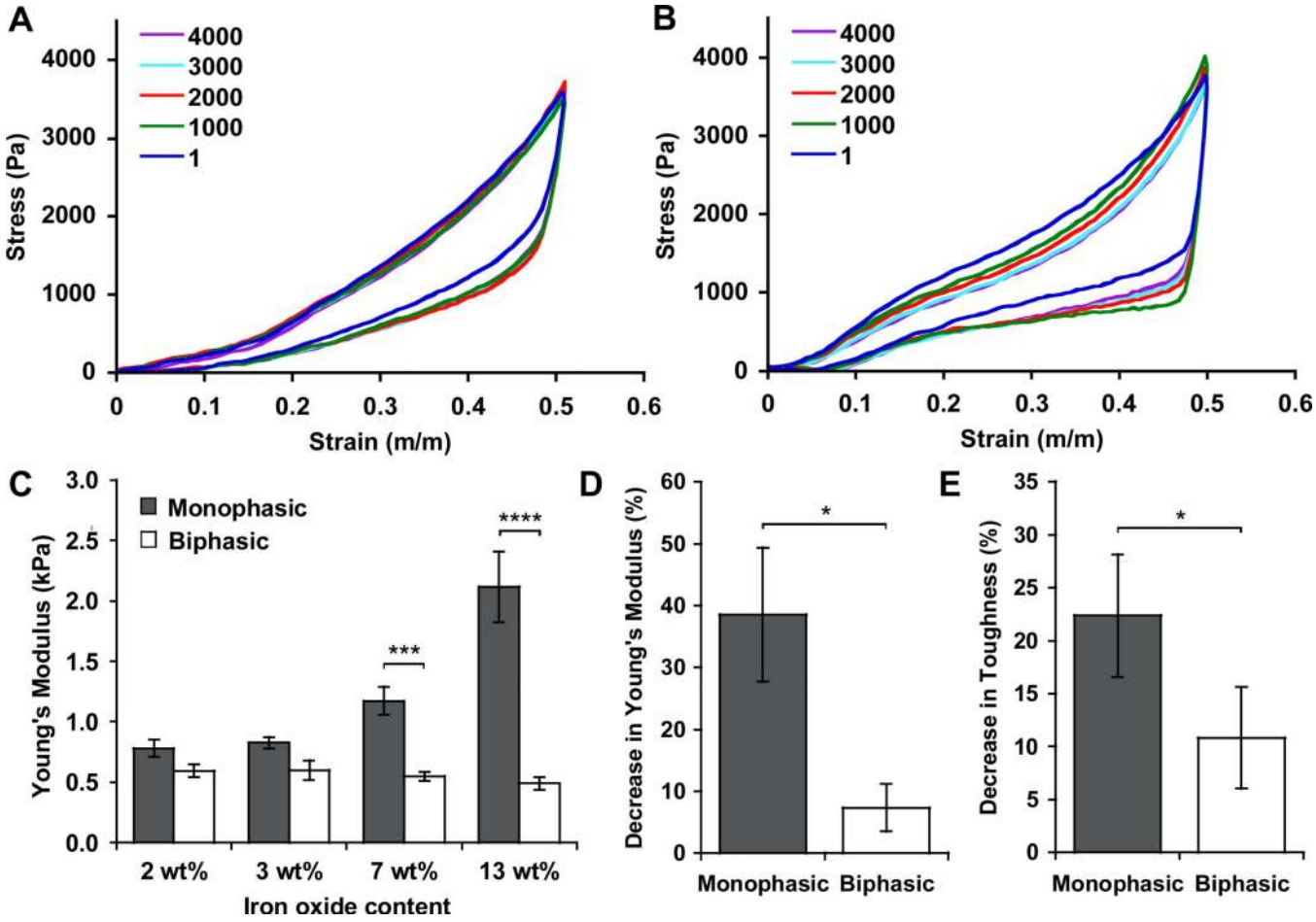

Figure 4.

Stress-strain curves for biphasic (A) and monophasic (B) ferrogels with 7 wt% iron oxide content undergoing 4000 compressions to 50% strain (every 1000th cycle displayed). (C) Initial Young's modulus of monophasic and biphasic ferrogels as a function of iron oxide content. Percent decrease in Young's modulus (D) and toughness at 50% strain (E) following 4000 cyclic compressions to 50% strain for monophasic and biphasic ferrogels, as compared to the values calculated from the first cycle of compression. Values represent the mean and standard deviation (n = 3–6). Data were compared using ANOVA with Bonferroni's post-hoc test in (C) and a two-tailed unpaired Student's t-test with Welch's correction in (D) and (E) (*$p < 0.05$, ***$p < 0.001$, ****$p < 0.0001$).

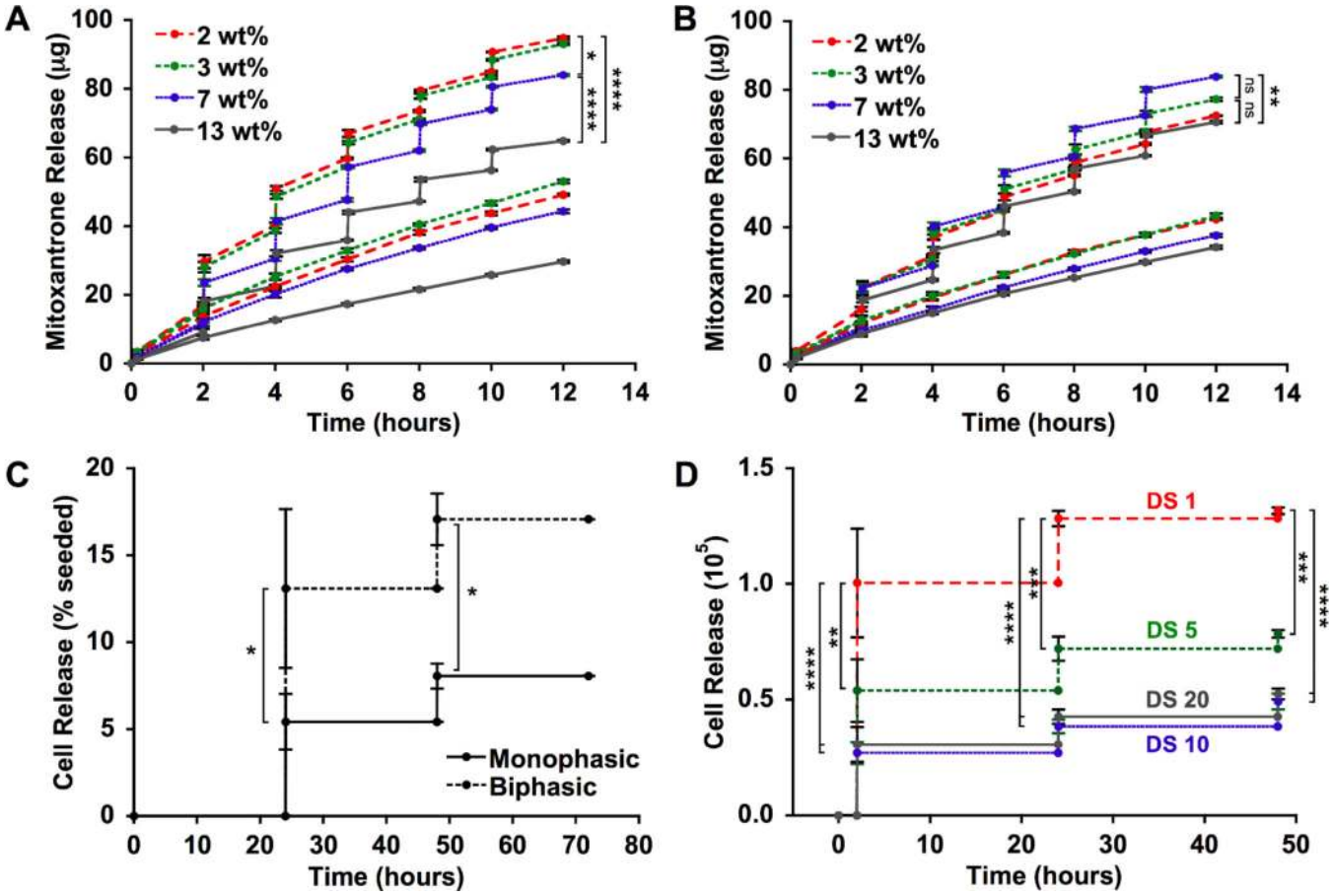

Figure 5.

Mitoxantrone release from biphasic (A) and monophasic (B) ferrogels following no stimulation (bottom curve) or magnetic field stimulation for 2 minutes at 1 Hz every 2 hours (top curve). All ferrogels were initially loaded with 150 μg mitoxantrone. (C) Viable cell release from 7 wt% DS10 (10RGD peptides per alginate chain) monophasic and biphasic ferrogels following magnetic field stimulation for 2 minutes at 1 Hz every 24 hours. (D) Viable cell release from biphasic ferrogels of varying RGD density following magnetic field stimulation for 2 minutes at 1 Hz every 24 hours. Viable cells were defined as cells excluding trypan blue. Values represent the mean and standard deviation ($n = 4$). Data were compared using ANOVA with Bonferroni's post-hoc test in (A), (B),and (D) and a two-tailed unpaired Student's *t*-test with Welch's correction in (C) (ns = not significant, *$p <$ 0.05, **$p < 0.01$, ***$p < 0.001$, ****$p < 0.0001$).

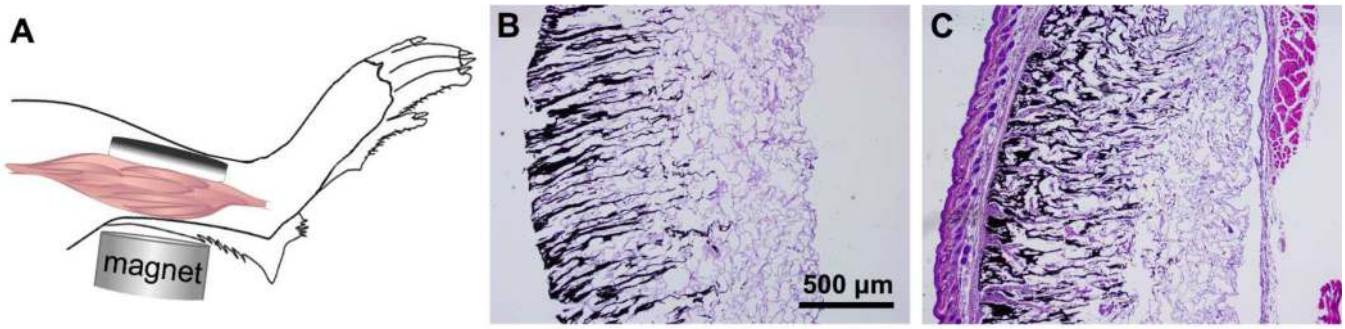

Figure 6.

(A) Schematic of biphasic ferrogel implant in mouse himdlimb depicting orientation of ferrogel relative to skin, muscle tissue, and magnet. Cross-sections of biphasic ferrogels stained with hematoxylin and eosin at 3 days (B) and 2 weeks (C) following implantation (n = 5).